

https://dspace.org/

Characterization of the 2D SuSchriefferHeeger Model with SecondNearestNeighbor Interactions

Chani Stella van Niekerk; Robert Warmbier

WILEY-V C H VERLAG GMBH
https://hdl.handle.net/10539/40475
WOS

Downloaded from a DSpace repository. https://dspace.org/

physica status solidi b
www.pss-b.com

Check for updates

Characterization of the 2D Su–Schrieffer–Heeger Model with Second-Nearest-Neighbor Interactions

Chani Stella van Niekerk and Robert Warmbier**

It is known that a 2D-dimerized Su–Schrieffer–Heeger model can produce a nontrivial topological phase. It is a simple nearest-neighbor model with four lattice sites in 2D. The Su–Schrieffer–Heeger model is easy to analyze but neglects important interaction in physical systems. Herein, an extended version of this model is proposed which includes all possible second-nearest-neighbor interactions in order to grant more flexibility when describing realistic systems. The addition of these interactions changes the symmetry of the model and as a result affects the topological properties. In order to characterize the topological changes to the model, a polarization invariant is used. It is further shown that these symmetry breaking interactions can be used to evoke a topological phase transition as well.

1. Introduction

The discovery of the quantum Hall effect in the 1980s led to the definition of a quantum state where the bulk of a sample (2D at the time) was insulating and the electric current was carried only along the edge of the sample. With the use of the concept of topology, this state could be defined as topologically distinct from all other states of matter known before this.[1]

Materials presenting this state were categorized as topological insulators and have been studied extensively since their discovery.[1–5] Topological insulators have a bulk bandgap like normal insulators; however, their edge states are conducting. The conducting states are by definition robust and thus resistant to defects and impurities provided the symmetry of the system is preserved.[2]

When a d-dimensional material is in a nontrivial topological state, it can host $(d-n)$ dimensional boundary states where $n = 1, \ldots, d-1$ when it exhibits chiral symmetry. For example, a 2D topological insulator can host 1D (conducting states along the border without the corners) and 0D (conducting states on the corners) conducting states.[6] For the sake of consistency, 0D and 1D states are called corners and edges, respectively. When $n > 1$, the topological insulator falls into the category of higher-order topological insulators (HOTIs). HOTIs are often weak topological insulators and have nontrivial phases that generally break down when disorder is added to them and evoke a symmetry change. Topological insulators are strong topological insulators when the edge and corner states are topologically protected from localization, and they are weak otherwise.[7]

In this work we characterize the nontrivial topological phase of a 2D extended Su–Schrieffer–Heeger (SSH) model with the addition of second-nearest-neighbor (SNN) interactions. The extended SSH model without SNN interactions has been studied extensively; in particular, it has been shown that this model exhibits both corner and edge states which are robust and nontrivial.[6–18] While most candidates for 2D topological materials have a hexagonal unit cell, not a rectangular one, there are exceptions, like $HfTe_5$ and $ZrTe_5$.[19] While the SSH model itself is very simple, it has far-reaching applications, for example, in the work done by Li et al.[18] a staggered version of this was used to describe the semimetal graphene. While in this work we study insulating materials, this illustrates the relevance of simple models to modeling real materials and forms a solid basis to build upon. Ivanova et al.[20] use an electric circuit realization of a small 2D SSH grid to prove the existence of corner states in the SSH model with SNN interactions. In the work done by Xu et al.[14] only intracellular interactions between the B and C sites are considered and studied numerically. Neither the symmetrically equivalent A to D interaction is included, nor any intercellular interactions. These numerical studies indicate that edge/corner states are realizable; however, they cannot be used to fully describe or predict the topological properties in parameter space. In real systems, long-range interactions are common and it is possible that SNN interactions are stronger than nearest-neighbor (NN) interactions depending on the materials making up the system. A staggered diagonal interaction could also be considered, leaving room for applications to materials with different symmetry groups. This makes SNN interactions a necessary

C. S. van Niekerk
Department of Physics
University of Johannesburg
P.O. Box 524, Auckland Park 2006, Johannesburg, South Africa
E-mail: robert.warmbier@wits.ac.za

R. Warmbier
School of Physics
University of the Witwatersrand
1 Jan Smuts Avenue, Braamfontein 2001, Johannesburg, South Africa
E-mail: csvanniekerk@uj.ac.za

The ORCID identification number(s) for the author(s) of this article can be found under https://doi.org/10.1002/pssb.202300241.

© 2023 The Authors. physica status solidi (b) basic solid state physics published by Wiley-VCH GmbH. This is an open access article under the terms of the Creative Commons Attribution-NonCommercial-NoDerivs License, which permits use and distribution in any medium, provided the original work is properly cited, the use is non-commercial and no modifications or adaptations are made.

DOI: 10.1002/pssb.202300241

© 2023 The Authors. physica status solidi (b) basic solid state physics published by Wiley-VCH GmbH

addition to a more realistic SSH model. Medina-Vázquez[21] studied the effect of symmetric and asymmetric SNN interactions and the kinds of corner states they can produce in square lattices with fourfold rotation symmetry. Their SNN terms are somewhat different from the ones used in this article but resemble closest the δ_{xy} term used in this work, see Equation (2). Their work focuses on the characterization of the corner states rather than characterization of the topological space, which is more the focus of this article.

2. Theoretical Model

In this article, the extended SSH model comprises a set of interacting 1D SSH arrays coupled together to form a 2D system, as shown in **Figure 1**. Each 1D array consists of dimerized lattices along the x-direction each with two sublattice sites separated by a distance d. The 2D system is built from coupling the chains in a similar way along the y-direction. In order to keep the system general, two different 1D chains are used—one with sublattice sites A and B and another with sublattice sites C and D, resulting in an ABCD lattice site unit cell. In this model, AB (AC) and CD (BD) hoppings are identical, respectively, so that the ABCD lattice cannot generally be reduced to an ABBA lattice.

2.1. Real Space Model

Using tight-binding principles, as with a 1D SSH model, the 2D system can be split into its NN and SNN interactions. The resultant real space Hamiltonian $H = H_{\mathrm{NN}} + H_{\mathrm{SNN}}$ consists of

$$\begin{aligned} H_{\mathrm{NN}} = \sum_{n,m}\Big\{ & [\gamma_x|A_{n,m}\rangle + \gamma_x'|A_{n+1,m}\rangle]\langle B_{n,m}| + \\ & [\gamma_x|C_{n,m}\rangle + \gamma_x'|C_{n+1,m}\rangle]\langle D_{n,m}| + \\ & [\gamma_y|A_{n,m}\rangle + \gamma_y'|A_{n,m+1}\rangle]\langle C_{n,m}| + \\ & [\gamma_y|B_{n,m}\rangle + \gamma_y'|B_{n,m+1}\rangle]\langle D_{n,m}| + \mathrm{h.c.}\Big\} \end{aligned} \tag{1}$$

and

$$\begin{aligned} H_{\mathrm{SNN}} = \sum_{n,m}\Big\{ & [\delta|A_{n,m}\rangle + \delta_x|A_{n-1,m}\rangle + \delta_y|A_{n,m-1}\rangle + \\ & \delta_{xy}|A_{n-1,m-1}\rangle]\langle D_{n,m}| + \\ & [\delta|B_{n,m}\rangle + \delta_x|B_{n-1,m}\rangle + \delta_y|B_{n,m+1}\rangle + \\ & \delta_{xy}|B_{n-1,m+1}\rangle]\langle C_{n,m}| + \mathrm{h.c.}\Big\} \end{aligned} \tag{2}$$

Here n, m refer to the index of the unit cells in the x and y directions, γ_l and γ_l'; $l \in \{x, y\}$ are the nearest intracell and intercell interactions, and δ and δ_p', $(p \in \{x, y, xy\})$, are the intracell and intercell SNN interactions. When $p = \{x, y\}$, the intercell hopping is across the edge of the unit cell and when $p = xy$, the hopping crosses the corner of the cell.

The real space system is studied using a finite number of repeated unit cells assuming both periodic and nonperiodic boundary conditions. Periodic boundary conditions are simulated by connecting the first and last cells in the chosen periodic direction, while nonperiodic boundary conditions are applied by leaving the first and last cells as free ends. In this work, we only study the nonperiodic and completely periodic cases, the case with mixed boundary conditions follows trivially from those.

For nonperiodic systems, the allowed states can be split into bulk, edge, and corner states when chiral symmetry is present. These states are defined on the localization of their probability density distribution. Similarly, when chiral symmetry is not present, border states localized on the corner and edge or a combination of the two are defined in the same way. This categorization allows the confirmation of the topological states which occur in the system. Edge planes can be chosen to align with the edges of the unit cell or cut through the center of the cell. For bipartite lattices these are not equivalent. Cutting through the center of the cell is equivalent to the shifts $\gamma_x \rightleftarrows \gamma_x'$, $\gamma_y \rightleftarrows \gamma_y'$, $\delta \rightleftarrows \delta_{xy}$, and $\delta_x \rightleftarrows \delta_y$. As this would belong to different topological states, as will be seen, the latter case is not considered here.

2.2. Reciprocal Space Model

Hermitian systems have a direct relation between the topological properties of the bulk reciprocal space system and the conducting edge/corner states in real space due to bulk boundary correspondence. By assuming the system is infinitely periodic and Fourier

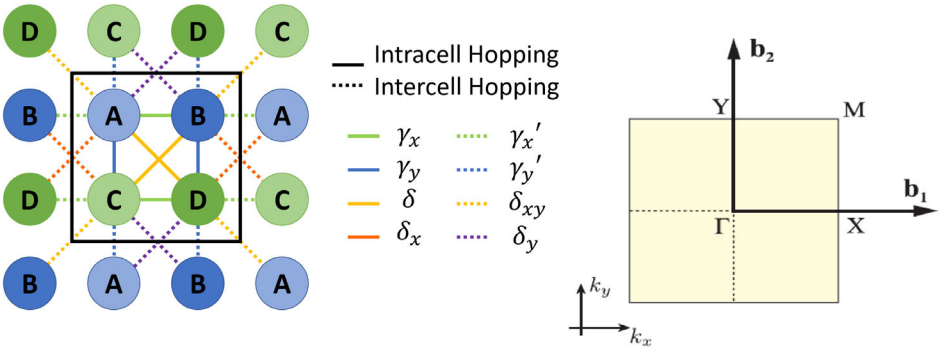


Figure 1. (Left) Construction of a 2D system using two different 1D SSH chains coupled together in the y-direction. Lattice sites A, B, C, and D represent one unit cell (outlined in black). Dashed and solid lines show all the possible nearest and next-nearest-neighbor hoppings from each unit cell. (Right) The typical 2D Brillouin zone for the unit cell in reciprocal space. Γ, M, X, and Y represent the high-symmetry points of the cell.

© 2023 The Authors. physica status solidi (b) basic solid state physics published by Wiley-VCH GmbH

15213951, 2024, 1, Downloaded from https://onlinelibrary.wiley.com/doi/10.1002/pssb.202300241 by University Of Wiwatersrand, Wiley Online Library on [27/08/2024]. See the Terms and Conditions (https://onlinelibrary.wiley.com/terms-and-conditions) on Wiley Online Library for rules of use; OA articles are governed by the applicable Creative Commons License

transforming the real-space Hamiltonian, Bloch-wave solutions of the form

$$|\psi(\vec{\mathbf{k}})\rangle = \sum_X \sum_{n,m} \left[e^{i\vec{\mathbf{k}}\cdot(n,m)} \phi_X(\vec{\mathbf{k}}) | X_{n,m} \rangle \right] \tag{3}$$

with $X \in \{A, B, C, D\}$ are found. Since $E\phi = h(\vec{\mathbf{k}})\phi$, the corresponding reciprocal space Hamiltonian in the basis $\hat{\psi}^{\dagger}_{\vec{\mathbf{k}}} = (\hat{A}, \hat{B}, \hat{C}, \hat{D})$ can be written as[22]

$$H = \hat{h}_{\mathrm{SSH}}(\vec{\mathbf{k}}) = \begin{pmatrix} 0 & s_x(k_x) & s_y(k_y) & s_{xy}(\vec{\mathbf{k}}) \\ s_x^*(k_x) & 0 & s'_{xy}(\vec{\mathbf{k}}) & s_y(k_y) \\ s_y^*(k_y) & s'^*_{xy}(\vec{\mathbf{k}}) & 0 & s_x(k_x) \\ s^*_{xy}(\vec{\mathbf{k}}) & s_y^*(k_y) & s_x^*(k_x) & 0 \end{pmatrix} \tag{4}$$

where $s_l(k_l) = \gamma_l + \gamma'_l e^{-ik_l}$, $l \in \{x, y\}$, $s_{xy}(\vec{\mathbf{k}}) = \delta + \delta_x e^{-ik_x} + \delta_y e^{-ik_y} + \delta_{xy} e^{-i(k_x+k_y)}$, and $s'_{xy}(\vec{\mathbf{k}}) = \delta + \delta_x e^{ik_x} + \delta_y e^{-ik_y} + \delta_{xy} e^{-i(-k_x+k_y)}$.

3. Properties of the Model

Due to bulk boundary correspondence, by studying the reciprocal space Hamiltonian, one can derive the topological properties of the overall system. In particular, one can establish for which regions of the parameter space the system will be topological. These properties are protected by a set of symmetries defined using the Hamiltonian.

In order for the topological state of an insulating system to change, a bandgap closure or band inversion needs to occur. The closure is a necessary, but insufficient, condition for the transition. To confirm that the topological phase changes, an invariant quantity derived from the Hamiltonian must accompany the gap closure.

Band inversions and invariant quantities can be defined for metallic systems as well; however, due to the large density of states in a small energy interval around the Fermi level, quantifying the change in phase is challenging to keep track of and is beyond the scope of this work.

3.1. Energy Eigenvalues

Gap closures act as an initial markers for a potential topological phase transition. Degeneracy in the bands can be found by setting the discriminant of the characteristic polynomial describing the energy eigenvalues to 0. The gap closure conditions describe the points in parameter space where the degeneracy occurs, but do not distinguish why a degeneracy occurs, making it a necessary but not sufficient condition for phase transition.

When SNN interactions are excluded, the energy values are given by

$$E = \pm \left| |s_x| \pm |s_y| \right| \tag{5}$$

In order for the valence and conduction bands to have the same energy, $\frac{\gamma'_l}{\gamma_l} = -e^{\pm ik_l}$, with $l \in \{x, y\}$. These conditions hold in parameter space for at least one k-value. For example, the conditions simplify to $\frac{\gamma'_l}{\gamma_l} = \pm 1$ for $k_l = 0, \pi$ and $\frac{\gamma_x \gamma'_x}{\gamma_y \gamma'_y} = \pm 1$ when $k_x = k_y = 0$ or π or $k_{x(y)} = 0$ and $k_{y(x)} = \pi$.

The addition of SNN interactions gives a more complicated system of energy eigenvalues of the form

$$\begin{aligned} E_{-\pm} &= -\tfrac{\sqrt{3}}{6}\left[\sqrt{A'_2} \pm \sqrt{B'_2 - C'_2}\right] \\ E_{+\pm} &= \tfrac{\sqrt{3}}{6}\left[\sqrt{A'_2} \pm \sqrt{B'_2 + C'_2}\right] \end{aligned} \tag{6}$$

where A'_2, B'_2, and C'_2 are listed in terms of the NN and SNN parameters in detail in the Supporting Information. For this model, meaningful analytical discriminant conditions cannot not be given for the general case; however, the form of the energy expression is indicative of symmetry breaking. Due to the C'_2 term, the system no longer has chiral or particle–hole symmetry.

3.2. Wave Functions

In order to fully define the topological phase transition, a gap closure needs to be accompanied by a change in an invariant quantity. Invariants are defined using the wave functions of the model Hamiltonian. For the general 2D SSH model without SNN interactions, the analytic wave function is expressed as follows.

$$\begin{aligned} \Psi_- &= \left\{ -\frac{\sqrt{s_x s_y}}{2\sqrt{s_x^* s_y^*}}, +(-)\frac{\sqrt{s_y}\,||s_x|-|s_y||}{2\sqrt{s_y^*}(|s_x|-|s_y|)}, -(+)\frac{\sqrt{s_x}\,||s_x|-|s_y||}{2\sqrt{s_x^*}(|s_x|-|s_y|)}, \frac{1}{2} \right\} \\ \Psi_+ &= \left\{ \frac{\sqrt{s_x s_y}}{2\sqrt{s_x^* s_y^*}}, -(+)\frac{\sqrt{s_y}\,||s_x|+|s_y||}{2\sqrt{s_y^*}(|s_x|+|s_y|)}, -(+)\frac{\sqrt{s_x}\,||s_x|+|s_y||}{2\sqrt{s_x^*}(|s_x|+|s_y|)}, \frac{1}{2} \right\} \end{aligned} \tag{7}$$

As with the energy expressions, adding SNN interactions makes the expressions more complicated.

$$\begin{aligned} \Psi_{-\pm} &= \frac{\left\{ \frac{r_{1\pm}}{q_{1\pm}}, \frac{n_{1\pm}}{q_{1\pm}}, -\frac{s_{1\pm}}{q_{1\pm}}, 1 \right\}}{\sqrt{\left|\frac{n_{1\pm}}{q_{\pm}}\right|^2 + \left|\frac{r_{1\pm}}{q_{1\pm}}\right|^2 + \left|\frac{s_{1\pm}}{q_{1\pm}}\right|^2 + 1}} \\ \Psi_{+\pm} &= \frac{\left\{ \frac{r_{2\pm}}{q_{2\pm}}, \frac{n_{2\pm}}{q_{2\pm}}, -\frac{s_{2\pm}}{q_{2\pm}}, 1 \right\}}{\sqrt{\left|\frac{n_{1\pm}}{q_{\pm}}\right|^2 + \left|\frac{r_{2\pm}}{q_{2\pm}}\right|^2 + \left|\frac{s_{2\pm}}{q_{2\pm}}\right|^2 + 1}} \end{aligned} \tag{8}$$

with $r_{1\pm}$, $q_{1\pm}$, $n_{1\pm}$, and $s_{1\pm}$ listed in the Supporting Information.

The forms of the wave functions are indicative of how the addition of parameters to a system complicates the analytic expressions.

3.3. Symmetry

The energy expressions indicate a symmetry change when comparing the model with and without SNN interactions. In order to choose an appropriate invariant calculation to apply to the system, the details of the symmetry must be known. While several symmetries can be defined for a system, choosing an appropriate invariant hinges on time-reversal ($TH(\vec{\mathbf{k}})T^{-1} = H(-\vec{\mathbf{k}})$), particle–hole ($PH(\vec{\mathbf{k}})P^{-1} = -H(-\vec{\mathbf{k}})$), chiral ($CH(\vec{\mathbf{k}})C^{-1} = -H(\vec{\mathbf{k}})$), and inversion ($\imath H(\vec{\mathbf{k}})\imath^{-1} = H(-\vec{\mathbf{k}})$) symmetries. For

© 2023 The Authors. physica status solidi (b) basic solid state physics published by Wiley-VCH GmbH

15213951, 2024, 1, Downloaded from https://onlinelibrary.wiley.com/doi/10.1002/pssb.202300241 by University Of Witwatersrand, Wiley Online Library on [27/08/2024]. See the Terms and Conditions (https://onlinelibrary.wiley.com/terms-and-conditions) on Wiley Online Library for rules of use; OA articles are governed by the applicable Creative Commons License

a spinless system, these symmetries are given by time-reversal: $T = \kappa$, particle–hole: $P = \sigma_z^{(x)} \otimes \sigma_z^{(y)} \kappa$, chiral: $C = \sigma_z^{(x)} \otimes \sigma_z^{(y)}$, and inversion: $\iota = \sigma_x^{(x)} \otimes \sigma_x^{(y)}$, where $\sigma_x^{(l)}$ and $\sigma_z^{(l)}$ correspond to Pauli matrices acting in the sublattice subspace in the $l = \{x, y\}$ directions, and k is the complex conjugation operator.

When SNN interactions are omitted, the system presents all four symmetries. The addition of any of the SNN interactions removes chiral and particle hole symmetry.

One commonly used way to categorize topological insulators is described using the Altland Zirnbauer classification of topological insulators.[23] Here only time-reversal, chiral, and particle–hole symmetries are used to describe if a system has a trivial or a topological phase or not. For different classifications, the model will have different topological properties due to symmetry breaking. Systems with all three symmetries, like the standard SSH model, are labeled BDI.[23] A loss of particle–hole and chiral symmetry results in the well-defined edge and corner states in the BDI class of systems, changing to a lowered symmetry AI class of systems, which only exhibit time-reversal symmetry. The AI system still presents edge and corner states, but they are no longer consistently localized in the bandgap of the system.

3.4. Invariant

When a system undergoes a gap closure, the pseudomomentum in reciprocal space of the system acts as a conserved parameter. This can be exploited to define an invariant which describes the topological phase of the system.

2D systems with time-reversal, particle–hole, and chiral symmetries (BDI systems) have a trivial 2D Chern number. However, due to the Hamiltonian of the BDI system being separable, a vectored version of the invariant can be formed from the Zak phase in each independent direction as these values are quantized.[8,10] This invariant is convenient to use when no SNN interactions are present.

The Zak phase in its component form ($l \in \{x, y\}$) is described by

$$Z_l(\vec{\mathbf{k}}) = -\frac{i}{\pi} \sum_{j=1}^{N_{\text{occ}}} \int_0^{2\pi} \left\langle u_j(\vec{\mathbf{k}}) \middle| \frac{\partial}{\partial k_l} \middle| u_j(\vec{\mathbf{k}}) \right\rangle \mathrm{d}k_l, \quad l = \{x, y\} \tag{9}$$

where j runs over all occupied bands, $\left|u_j(\vec{\mathbf{k}})\right\rangle$ is the periodic Bloch function for the j^{th} band, and $\left\langle u_j(\vec{\mathbf{k}}) \middle| \frac{\partial}{\partial k_l} \middle| u_j(\vec{\mathbf{k}}) \right\rangle$ is the Berry connection. This value indicates the topological phase, $Z_l = 0$ indicates a trivial phase, while $Z_l = 2$ indicates a topological phase in each direction respectively.

If the system has inversion symmetry as well, the integral of the Zak phase can be reduced to the contributions at the four time reversal invariant momenta,[24] that is, $\Gamma(\vec{\mathbf{k}} = (0,0))$, $X(\vec{\mathbf{k}} = (\pi,0))$, $Y(\vec{\mathbf{k}} = (0,\pi))$, and $M(\vec{\mathbf{k}} = (\pi,\pi))$. This can be exploited to define a new invariant using the inversion eigenvalues at each point for the occupied bands. These eigenvalues are calculated using the matrix $\iota H \iota^{-1}$, where ι is the unitary inversion operator. The inversion eigenvalues can only take on values of ± 1, indicating if the bands have even or odd parity at each point.[25,26] Due to the symmetry present in the system, the product of the inversion eigenvalues at the high-symmetry points is always trivial, the Γ and M points always have the same parity eigenvalue. This can be exploited to form a vectored invariant.

$$\begin{aligned} (-1)^{\nu_x} &= \prod_{n_{\text{occ}}} \frac{\xi(X)}{\xi(\Gamma)} \\ (-1)^{\nu_y} &= \prod_{n_{\text{occ}}} \frac{\xi(Y)}{\xi(\Gamma)} \end{aligned} \tag{10}$$

This invariant is consistent with the vectored Zak phase for the system with no SNN interactions. Since the SNN interactions break chiral and particle–hole symmetry, the Zak phase is no longer well defined for this model. The alternate invariant is defined using only inversion and time-reversal symmetry, so it can still be used to describe the topological properties of the system and will therefore be used throughout this work. Since the SNN interactions break chiral and particle–hole symmetry, it should be noted that while the invariant is used for the BDI and AI models, it does not necessarily describe the same topological phase.

Using the wave functions listed in Equation (7) and the invariant at the high-symmetry points, it is found that a direction will be topological when $|\frac{\gamma_l'}{\gamma_l}| > 1$ when $l \in \{x, y\}$. Naturally since the expressions for the wave functions including SNN interactions (Equation (8)) are much less straight forward, these conditions are not so readily obtained. When considering only the high-symmetry points, the energy and inversion eigenvalues are as follows.

$$\begin{aligned} E_{1(2)}(\Gamma) &= \pm(\delta + \delta_x + \delta_{xy} + \delta_y - \gamma_x - \gamma_x') - \gamma_y - \gamma_y' \\ \xi_{1(2)}(\Gamma) &= \pm 1 \\ E_{3(4)}(\Gamma) &= \pm(-\delta - \delta_x - \delta_{xy} - \delta_y - \gamma_x - \gamma_x') + \gamma_y + \gamma_y', \\ \xi_{3(4)}(\Gamma) &= \pm 1 \\ \\ E_{1(2)}(X) &= \pm(-\delta + \delta_x + \delta_{xy} - \delta_y + \gamma_x - \gamma_x') - \gamma_y - \gamma_y', \\ \xi_{1(2)}(X) &= \pm 1 \\ E_{3(4)}(X) &= \pm(\delta - \delta_x - \delta_{xy} + \delta_y + \gamma_x - \gamma_x') + \gamma_y + \gamma_y', \\ \xi_{3(4)}(X) &= \pm 1 \\ \\ E_{1(2)}(Y) &= \pm(-\delta - \delta_x + \delta_{xy} + \delta_y - \gamma_x - \gamma_x') + \gamma_y - \gamma_y', \\ \xi_{1(2)}(Y) &= \pm 1 \\ E_{3(4)}(Y) &= \pm(\delta + \delta_x - \delta_{xy} - \delta_y - \gamma_x - \gamma_x') - \gamma_y + \gamma_y', \\ \xi_{3(4)}(Y) &= \pm 1 \end{aligned} \tag{11}$$

Using these expressions, depending on the parameter values, the above expressions could be used to establish the occupied bands and the ratio of their inversion eigenvalues, that is, the invariant. A phase transition is possible at any of these high-symmetry points, which means that SNN interactions can trigger a phase change.

4. Results

The bandgap and band behavior in reciprocal space give an indication of where a topological phase transition will occur. A topological phase should correspond to the localization of the probability density of an open system's real space wave functions.

Using these markers, a system with no SNN interactions will be studied to establish topological phases which warrant the addition of SNN perturbation. SNN interactions are then added to

© 2023 The Authors. physica status solidi (b) basic solid state physics published by Wiley-VCH GmbH

15213951, 2024, 1, Downloaded from https://onlinelibrary.wiley.com/doi/10.1002/pssb.202300241 by University Of Wiwatersrand, Wiley Online Library on [27/08/2024]. See the Terms and Conditions (https://onlinelibrary.wiley.com/terms-and-conditions) on Wiley Online Library for rules of use; OA articles are governed by the applicable Creative Commons License

each phase to reduce the symmetry of the system and thereby test the resilience of the topological phases under symmetry breaking perturbations.

4.1. 2D SSH Model

The gap conditions for the reciprocal space and real space systems should be similar for the large enough system due to bulk boundary correspondence. A system size of at least 65 × 65 unit cells was the smallest system required to still be representative of the k-space gaps. For localization checks in the open-boundary case, the border of the cell was assumed to be 4 unit cells thick.

The gap size for the periodic system for a given set of parameters was calculated to establish regions in parameter space where topological transitions could be possible. As this is a preliminary system, the smallest degrees of freedom are desired. When studying a purely isotropic model, $\gamma_x = \gamma_y$ and $\gamma'_x = \gamma'_y$, it was found that the system was always metallic. Metallic states are problematic to define topologically as the invariant is affected by the interaction of the bands and changes in their parity. While starting with a metallic phase and adding SNN interactions to cause a nonmetallic phase which is well defined topologically is not problematic, it limits the study. In order to ensure that all cases of the model are well represented, a "nearly isotropic" model is considered, where $\gamma_x = \gamma_y = \gamma$ and γ'_x and γ'_y are allowed to differ. In order to reduce the parameters, we scale all other parameters by γ, without loss of generality.

Figure 2 (top) indicates that the near-isotropic setup can describe both a metallic (blue region) and nonmetallic (yellow region) system. The localization of the nonperiodic wave functions of the valence band maximum (VBM) (Figure 2 (middle)) shows that the wave functions are localized in the bulk, edge, or at the corners in distinct regions of the parameter space. The white points represent points in parameter space where the localization of the wave functions was not numerically well defined. The right panel of the figure shows the corresponding parity invariant, which confirms the analytic results predicted by the discriminant conditions. When $\frac{\gamma'_l}{\gamma_l} < 1$, when l is x or y, the system is trivial and when $\frac{\gamma'_l}{\gamma_l} > 1$, the system is topological. At the topological transition point, that is, $\frac{\gamma'_l}{\gamma_l} = 1$, this value is not defined giving the white lines shown in the figure. These results show that when the system is topological in both directions, the corner state is preserved despite the metallicity of the system. For a partially trivial system, the metallic system shows a bulk localization, while the nonmetallic system shows the corner state predicted by the invariant. This serves as an example of why a metallic system and the localization of its states can be challenging to describe using an invariant quantity. The trivial topological phase always corresponds to a bulk metallic system. The lines forming the cross in the top panel correspond to lines in the invariant which do not behave as predicted by the regions surrounding them. This exemplifies why calculating a topological invariant for a metallic system is challenging. When there are numerous bands near the Fermi level, counting the number of parity changes numerically can result in the incorrect value.

These results allow the identification of three distinct topological phases, trivial: $(\nu_x, \nu_y) = (0,0)$, partially trivial: $(\nu_x, \nu_y) = (0,1)$ or $(1,0)$, and topological: $(\nu_x, \nu_y) = (1,1)$. These can further be broken down into metallic and nonmetallic cases where applicable. These distinctions led to the choice of five representative points in parameter space, indicated by stars in

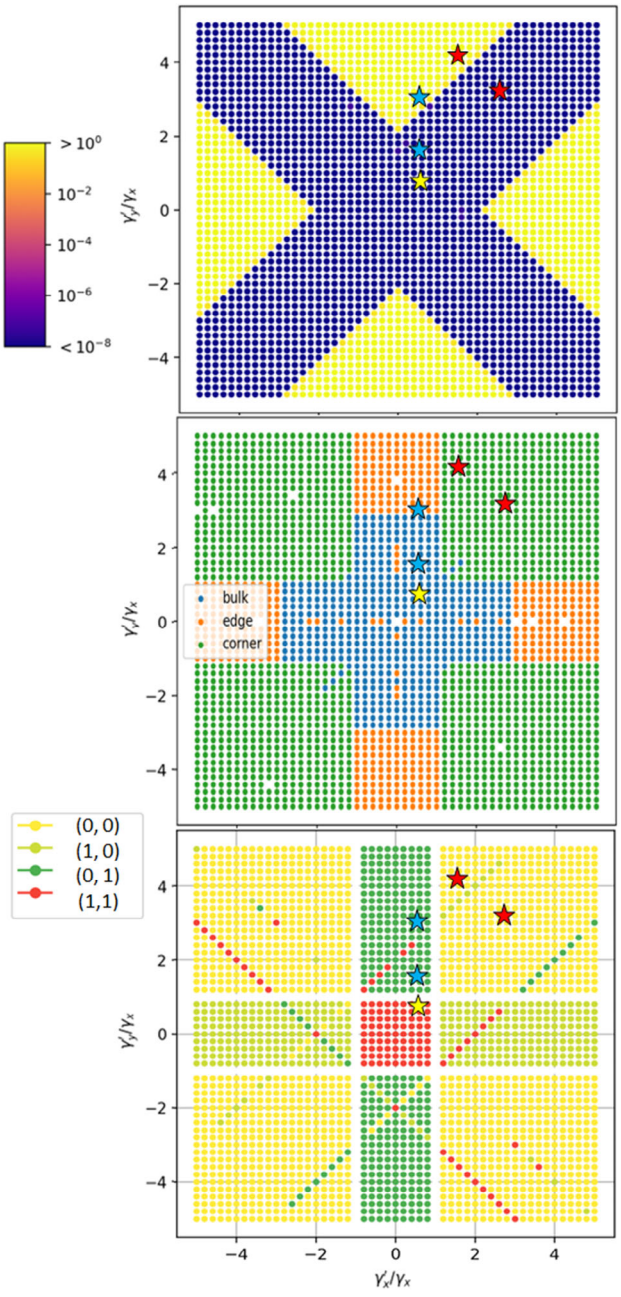


Figure 2. (Top) Bulk bandgap where the color bar on the left tracks the size of the bandgap, from blue (zero bandgap) to yellow (gap size >1). (Middle) VBM localization type for a system with 80 × 80 unit cells with open-boundary conditions, where blue, orange, and green represent a bulk, edge, and corner localization, respectively. (Bottom) Parity invariant for a nearly isotropic 2D SSH system, where 0 corresponds to a topological phase and 1 corresponds to a trivial phase. The stars represent the five different sample points used to study the different phases possible for the system.

© 2023 The Authors. physica status solidi (b) basic solid state physics published by Wiley-VCH GmbH

15213951, 2024, 1, Downloaded from https://onlinelibrary.wiley.com/doi/10.1002/pssb.202300241 by University Of Witwatersrand, Wiley Online Library on [27/08/2024]. See the Terms and Conditions (https://onlinelibrary.wiley.com/terms-and-conditions) on Wiley Online Library for rules of use; OA articles are governed by the applicable Creative Commons License

Figure 2. The points consist of a metallic, trivial phase (M_{00}) with $\gamma_x' = 0.5, \gamma_y' = 0.75$ (blue star), metallic and nonmetallic, partially trivial phases: M_{01} with $\gamma_x' = 0.5$, NM_{01} with $\gamma_y' = 1.6$, $\gamma_x' = 0.5, \gamma_y' = 3$ (yellow stars), and a metallic and nonmetallic topological phase: M_{11}, with $\gamma_x' = 2.5, \gamma_y' = 3.2$ and NM_{11} with $\gamma_x' = 1.5, \gamma_y' = 4.2$ (red stars).

4.2. 2D SSH Model with SNN Interactions

The addition of SNN interactions breaks chiral and particle–hole symmetry, evoking a change in the topological behavior of the system. In fact, the states are no longer well defined and will instead be labeled as nonbulk states localized on the edge, corner, or a combination of the two.

4.2.1. Single-Parameter Symmetry Breaking

To test the effect of SNN interactions on the states, they are added to a system with $\gamma_x' = 4.1$, while γ_y' and the SNN interaction are allowed to vary. This line is chosen so that a topological and partially topological phase are sampled. The results of the SNN additions are shown in **Figure 3**. γ_y' is varied on the horizontal axis, and one SNN parameter is varied on the vertical axis. The other SNN parameters are kept 0, respectively.

Focusing only on the nonmetallic regions (where the gap size is nonzero, i.e., the nonblue regions) shows that the addition of SNN interactions can—but does not have to—evoke an immediate change in the invariant, which is consistent with the perturbation causing a symmetry change. In general, the VBM state localization is consistent with what is expected from the invariant. The states do not always have a one-to-one correlation with the invariant, this is believed to be due to finite size effects.

To demonstrate a typical example, we choose the topological NM_{11} configuration and a $\delta = -0.8$ SNN interaction. This configuration is nonmetallic in the bulk, while the open-boundary system is gapless. In **Figure 4** (top), the energy eigenvalues and their localization character are shown for several system sizes. The zero-energy corner states are still present and unchanged. The SNN term deforms and shifts the bulks though, so that the VBM now sits above these states at $E_{\mathrm{VBM}} = 0.1$. This can also be seen in the band structure plot in Figure 4 (center). This system also shows low-energy edge states in the bulk gap. The corner and edge states are barely affected by the symmetry

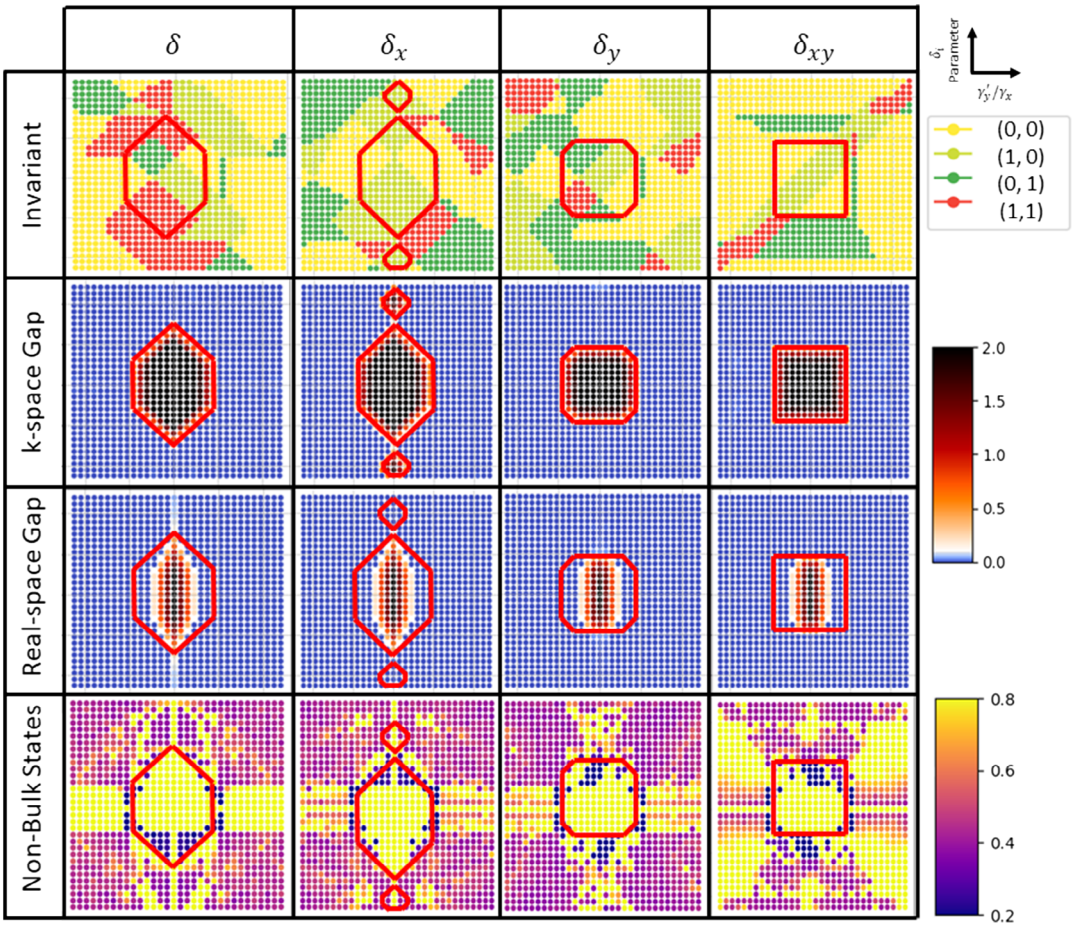


Figure 3. (Top row) Bulk invariant, (second row) reciprocal space gap size, (third row) real space gap size, and (bottom row) VBM state localization for a nonperiodic real system. The plots are made for $\gamma_x' = 4.1$ and consider the relationship between each of the different SNN parameters as a function of γ_y'. Parameters are varied in interval $[-5, 5]$. An invariant value of 1 or 0 refers to a trivial or topological phase, respectively. The first color bar runs from blue to black, indicating gaps from 0.0 to 2.0. The last color bar represents the magnitude of the VBM localization.

© 2023 The Authors. physica status solidi (b) basic solid state physics published by Wiley-VCH GmbH

15213951, 2024, 1, Downloaded from https://onlinelibrary.wiley.com/doi/10.1002/pssb.202300241 by University Of Witwatersrand, Wiley Online Library on [27/08/2024]. See the Terms and Conditions (https://onlinelibrary.wiley.com/terms-and-conditions) on Wiley Online Library for rules of use; OA articles are governed by the applicable Creative Commons License

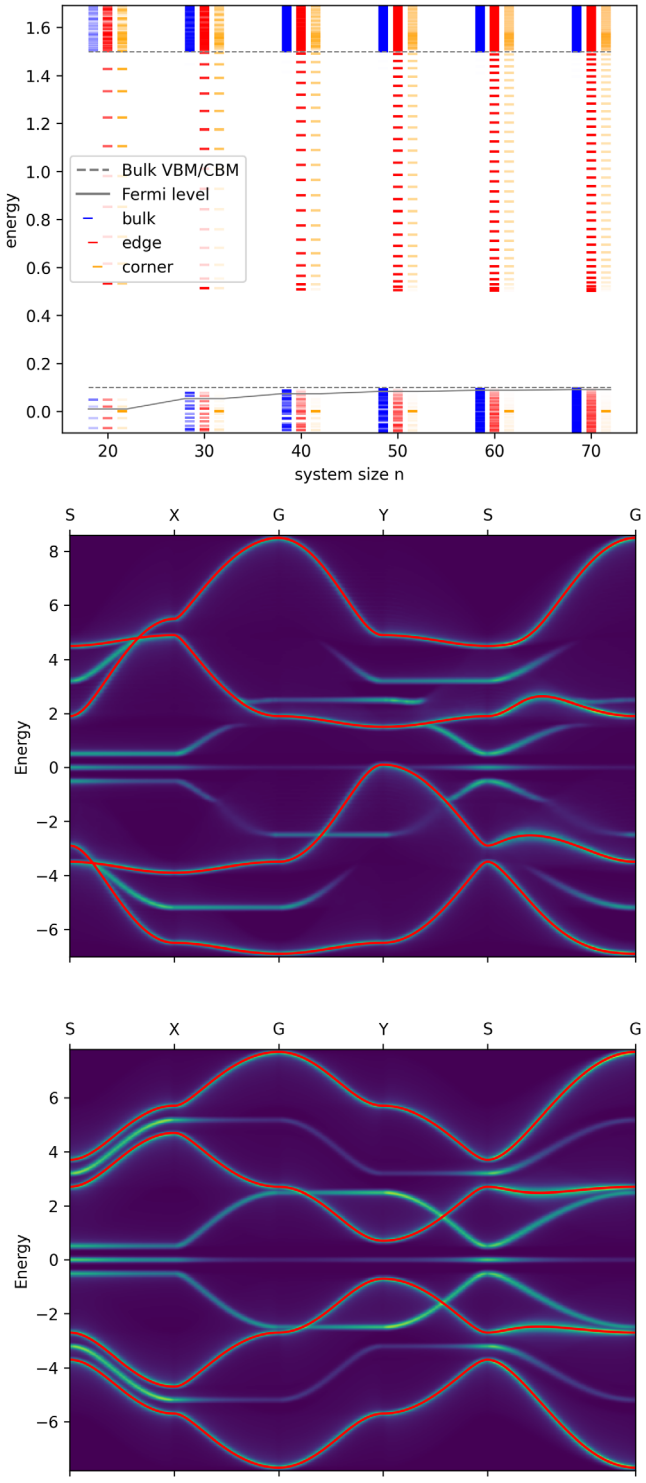


Figure 4. Fully topological nonmetallic phase, where $\gamma_x = \gamma_y = 1$, $\gamma'_x = 1.5$, and $\gamma'_y = 4.2$ with $\delta = -0.8$. Top: Eigenvalues and state localization for different system sizes and open-boundary conditions. Opacity indicates strength of bulk, edge, and corner contributions to the wave functions. Center: Fourier transform of $n = 70$ wave functions. Red curves represent the corresponding bulk band structure. Bottom: Reference band structure without SNN interaction.

breaking SNN interaction and retain their energy and dispersion from the SSH reference state, Figure 4 (bottom).

4.2.2. Two-Parameter Variations

With the confirmation that the symmetry breaking caused by a single SNN interaction causes a phase change, a combination of two of the parameters is now introduced for each representative point. We would like to investigate a small symmetry perturbation on the system, so to limit the effect on the symmetry of the system, δ-δ_{xy} and δ_x-δ_y were studied as pairs so that there are contributions in both directions.

Since the study focuses on the changes due to the SNN interactions, the role of symmetry in this process is important to note. When one of the representative points describing the different states is chosen, the system behaves in a qualitatively consistent way in that region irrespective of the exact parameters of the point chosen. Along the diagonal, the high symmetry results in the invariant being ill-defined. These diagonals correspond to the transition lines predicted by the analytic invariant conditions.

For illustrative purposes, we discuss the δ-δ_{xy} pair. The δ_x-δ_y results are shown in the Supporting Information. The first two columns of **Figure 5** indicate that, aside from the fully topological metallic state, a gap can be closed or opened by the parameter pair. Both the invariant and conducting state localization are defined using the VBM. Due to the interaction between the bands near the Fermi level in a metallic system, different tools beyond the scope of this work are required to study these states. The last two columns of Figure 5 show that the insulating regions are topologically protected. When the region is insulating in the bulk, but only a subset of that region is insulating in the open-boundary system, a conducting edge/corner state (confirmed by the invariant) is visible. This exemplifies how the bulk gap closure is necessary, but does not always indicate a topological phase transition. Due to the finite size effect, the VBM localization does not fully correspond to the invariant, but would for a larger enough system size. When the symmetry of the Hamiltonian, and by implication the bands, is broken, the distinction between edge and corner states is no longer clearly defined. Due to this, we choose to define the topological phases when SNN interactions are included as topologically protected (edge/corner localized, green or yellow) or trivial (bulk localized, red). While the edge/corner localization is no longer the distinguishing factor between the green and yellow regions due to the change in symmetry, they now distinguish a different topological property.

To exemplify this difference, a Fourier transform of the open-boundary wave functions was plotted over reciprocal space and compared to the bulk wave functions. In order for a topologically protected conducting state to be well defined, it should be in the bulk bandgap. Provided, the region where the gap size of the open-boundary system is less than or equal to the bulk bandgap, the topological state is well defined and in the gap. For example, the top panel of **Figure 6** shows an example of where the state is in the bulk band gap, that is, $\delta = 0.6$ and $\delta_{xy} = 0.3$ and well defined (yellow region). This corresponds to a fully topological system where the entire edge state is in the bandgap. The bottom panel of Figure 6 with $\delta = -0.9$ and $\delta_{xy} = 0.95$ corresponds to a

© 2023 The Authors. physica status solidi (b) basic solid state physics published by Wiley-VCH GmbH

15213951, 2024, 1, Downloaded from https://onlinelibrary.wiley.com/doi/10.1002/pssb.202300241 by University Of Witwatersrand, Wiley Online Library on [27/08/2024]. See the Terms and Conditions (https://onlinelibrary.wiley.com/terms-and-conditions) on Wiley Online Library for rules of use; OA articles are governed by the applicable Creative Commons License

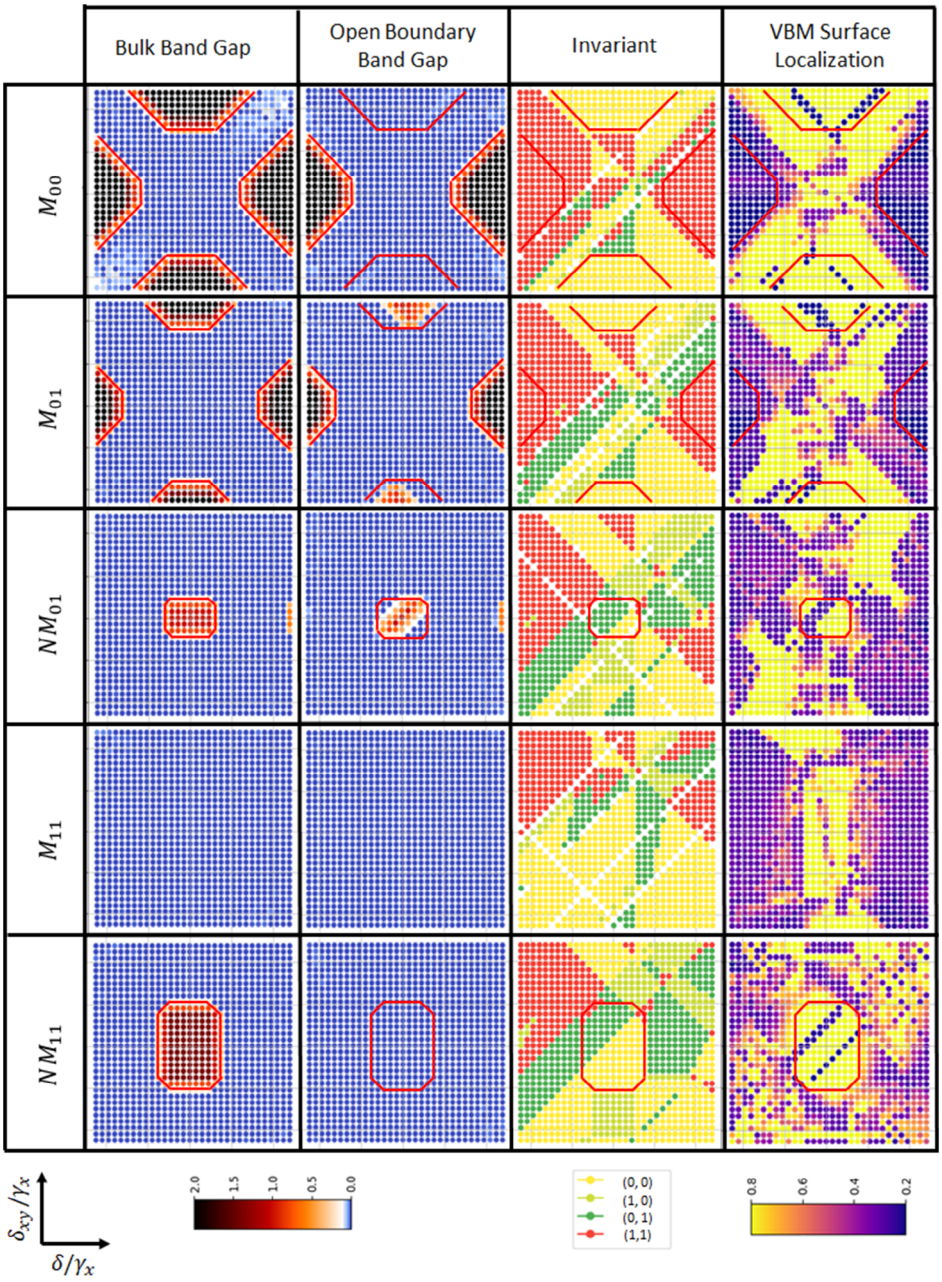


Figure 5. The bulk bandgap, open-boundary bandgap, invariant, and VBM localization for an initially metallic trivial and partially topological phase and a nonmetallic trivial, partially and completely topological phase for varying δ and δ_{xy}. The left color bar represents a gap running from 0 (blue) to 2.0 (black). The right color bar represents the magnitude of the VBM localization.

partially topological phase where only part of the edge/corner states are in the bandgap (green region). A trivial phase would have no edge/corner states in the bandgap at all.

5. Conclusion

The addition of SNN interaction to a 2D SSH model removes chiral and particle–hole symmetry, changing the topological classification from BDI and AI. For this case, a vectorized parity invariant can be defined and the parity eigenvalues for this model are given.

In this model, SNN interactions have little or no effect on the presence of the initial edge/corner states. They do however shift and deform the bulk bands, changing their localization on the edges as well as where they are in the bandgap. This evokes a change from a strong to a weak topological phase for a small value of the parameter set due to band inversions and shifts of the edge/corner states in and out of the bandgap. For larger parameter values, it is possible to evoke a change allowing a

© 2023 The Authors. physica status solidi (b) basic solid state physics published by Wiley-VCH GmbH

15213951, 2024, 1, Downloaded from https://onlinelibrary.wiley.com/doi/10.1002/pssb.202300241 by University Of Witwatersrand, Wiley Online Library on [27/08/2024]. See the Terms and Conditions (https://onlinelibrary.wiley.com/terms-and-conditions) on Wiley Online Library for rules of use; OA articles are governed by the applicable Creative Commons License

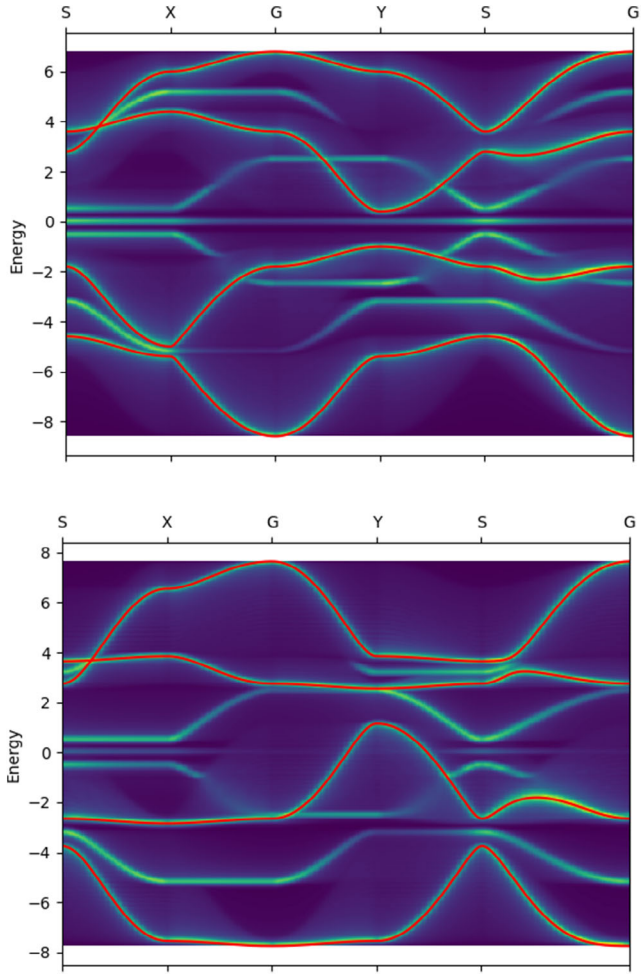


Figure 6. Fourier transforms of the open-boundary wave functions plotted over reciprocal space, with the bulk wave functions indicated in red for a NM_{11} system, where the bulk bandgap is less than the open-boundary bandgap, with (top) $\delta = 0.6$ and $\delta_{xy} = 0.3$, that is, a fully topological phase, and (bottom) $\delta = -0.9$ and $\delta_{xy} = \pm 0.95$, that is, a partially topological phase. A system size of $n = 60$ was used.

transition from a metallic to a nonmetallic system and also from a topological phase to a trivial one or vice versa.

We find that the nonmetallic fully topological phase (NM_{11}) is most resilient against the symmetry-breaking perturbation. New topological phases for larger magnitudes of SNN interaction occur in particular for the trivial (M_{00}) and partially trivial (M_{01}) metallic phases.

Supporting Information

Supporting Information is available from the Wiley Online Library or from the author.

Acknowledgements

The support of the DSI-NRF Centre of Excellence in Strong Materials (CoE-SM) toward this research is hereby acknowledged. Opinions expressed and conclusions arrived at are those of the author and are not necessarily to be attributed to the CoE-SM. R.W. also acknowledges support by the Mandelstam Institute for Theoretical Physics.

Conflict of Interest

The authors declare no conflict of interest.

Data Availability Statement

The data that support the findings of this study are available in the supplementary material of this article.

Keywords

model Hamiltonians, Su–Schrieffer–Heeger, topological insulators

Received: May 26, 2023
Revised: November 1, 2023
Published online: November 20, 2023

[1] X.-L. Qi, S.-C. Zhang, *Rev. Mod. Phys.* **2011**, *83*, 1057.
[2] M. Z. Hasan, C. L. Bern, *Rev. Mod. Phys.* **2010**, *82*, 3045.
[3] B. A. Bernevig, T. L. Hughes, S.-C. Zhang, *Science* **2006**, *314*, 1757.
[4] J. E. Moore, *Nature* **2010**, *464*, 194.
[5] C. L. Kane, E. J. Mele, *Phys. Rev. Lett.* **2005**, *95*, 226801.
[6] Z.-G. Chen, C. Xu, R. Al Jahdali, J. Mei, Y. Wu, *Phys. Rev. B* **2019**, *100*, 075120.
[7] A. Coutant, V. Achilleos, O. Richoux, G. Theocharis, V. Pagneux, *Phys. Rev. B* **2020**, *102*, 214204.
[8] F. Liu, K. Wakabayashi, *Phys. Rev. Lett.* **2017**, *118*, 076803.
[9] F. Liu, H.-Y. Deng, K. Wakabayashi, *Phys. Rev. B* **2018**, *97*, 035442.
[10] D. Obana, F. Liu, K. Wakabayashi, *Phys. Rev. B* **2019**, *100*, 075437.
[11] B.-Y. Xie, H.-F. Wang, H.-X. Wang, X.-Y. Zhu, J.-H. Jiang, M.-H. Lu, Y.-F. Chen, *Phys. Rev. B* **2018**, *98*, 205147.
[12] Y. Ota, F. Liu, R. Katsumi, K. Watanabe, K. Wakabayashi, Y. Arakawa, S. Iwamoto, *Optica* **2019**, *6*, 786.
[13] W. Zhu, G. Ma, *Phys. Rev. B* **2020**, *101*, 161301.
[14] X.-W. Xu, Y.-Z. Li, Z.-F. Liu, A.-X. Chen, *Phys. Rev. A* **2020**, *101*, 063839.
[15] W. A. Benalcazar, A. Cerjan, *Phys. Rev. B* **2020**, *101*, 161116.
[16] M. Kim, J. Rho, *Nanophotonics* **2020**, *9*, 3227.
[17] R. W. Bomantara, L. Zhou, J. Pan, J. Gong, *Phys. Rev. B* **2019**, *99*, 045441.
[18] C.-A. Li, S.-J. Choi, S.-B. Zhang, B. Trauzettel, *Phys. Rev. Res.* **2022**, *4*, 023193.
[19] Z. Fan, Q.-F. Liang, Y. Chen, S.-H. Yao, J. Zhou, *Sci. Rep.* **2017**, *7*, 45667.
[20] P. A. Ivanova, N. A. Olekhno, V. I. Kachin, D. V. Zhirihin, P. S. Seregin, M. A. Gorlach, *J. Phys.: Conf. Ser.* **2020**, *1695*, 012142.
[21] J. A. Medina-Vázquez, *Phys. Rev. A* **2023**, *107*, 043503.
[22] C. S. van Niekerk, R. Warmbier, *Phys. Status Solidi B* **2023**, *260*, 2300018.
[23] S. Ryu, A. P. Schnyder, A. Furusaki, A. W. W. Ludwig, *New J. Phys.* **2010**, *12*, 065010.
[24] L. Fu, C. L. Bern, *Phys. Rev. B* **2007**, *76*, 045302.
[25] T. L. Hughes, E. Prodan, B. A. Bernevig, *Phys. Rev. B* **2011**, *83*, 245132.
[26] C. Fang, M. J. Gilbert, B. A. Bernevig, *Phys. Rev. B* **2012**, *86*, 115112.

© 2023 The Authors. physica status solidi (b) basic solid state physics published by Wiley-VCH GmbH

15213951, 2024, 1, Downloaded from https://onlinelibrary.wiley.com/doi/10.1002/pssb.202300241 by University Of Witwatersrand, Wiley Online Library on [27/08/2024]. See the Terms and Conditions (https://onlinelibrary.wiley.com/terms-and-conditions) on Wiley Online Library for rules of use; OA articles are governed by the applicable Creative Commons License